Atmospheric
Chemistry
and Physics
Discussions

Investigation of Aerosol-Cloud Interactions under Different Absorptive Aerosol Regimes using ARM SGP Ground-Based Measurements

Xiaojian Zheng[1], Baike Xi[1], Xiquan Dong[1], Timothy Logan[2], Yuan Wang[3,4] and Peng Wu[1]

5

[1]Department of Hydrology and Atmospheric Sciences, University of Arizona, Tucson, AZ, USA
[2]Department of Atmospheric Sciences, Texas A&M University, College Station, TX, USA
[3]Division of Geological and Planetary Sciences, California Institute of Technology, Pasadena, CA, USA
10 [4]Jet Propulsion Laboratory, California Institute of Technology, Pasadena, CA, USA

Correspondence to: Baike Xi (baikex@email.arizona.edu)

15   **Abstract.** The physicochemical properties of aerosols and their impacts on cloud microphysical properties are examined using data collected from the Department of Energy Atmospheric Radiation Measurement (ARM) facility over the Southern Great Plains region of the United States (ARM-SGP). A total of 16 low-level stratus cloud cases under daytime coupled boundary layer conditions are selected. The aerosol-cloud interaction index (ACI_r) is

20   used to quantify the aerosol impacts with respect to cloud-droplet effective radius. The mean value of ACI_r calculated from all selected samples is 0.145 ± 0.05 and ranges from 0.09 to 0.24 at a range of cloud liquid water paths (LWP=20-300 g m^{-2}). The magnitude of ACI_r decreases with increasing LWP which suggests a cloud microphysical response to diminished aerosol loading presumably due to enhanced collision-coalescence processes and enlarged

25   particle size. In the presence of weak light-absorbing aerosols, the low-level clouds feature a higher number concentration of cloud condensation nuclei (N_{CCN}) and smaller effective radii (r_e) while the opposite is true for strong light-absorbing aerosols. Furthermore, the mean activation ratio of aerosols to CCN (N_{CCN}/N_a) for weakly (strongly) absorbing aerosols is 0.54 (0.45), owing to the different hygroscopic abilities associated with the dominant aerosol species.

30   In terms of the sensitivity of cloud droplet number concentration (N_d) to aerosol loading, the conversion ratio of N_d/N_{CCN} for weakly (strongly) absorptive aerosols is 0.68 (0.54).

Consequently, we expect larger shortwave radiative cooling effect from clouds influenced by weakly absorbing aerosols than strongly absorbing aerosols.

1   Introduction

5   Clouds play a critical role in the Earth's climate by acting as the dominant modulator of radiative transfer in the atmosphere and have substantial impacts on the global climate. The radiative effect of clouds contributes to one of the largest uncertainties in climate modeling (IPCC, 2013), and has been well known to be influenced by aerosol loading. An increase in aerosol concentration can lead to the enhancement of cloud droplet number concentration (N_d)

10   and the reduction of cloud droplet effective radii (r_e), which results in an increase of cloud albedo. This phenomenon is defined as the aerosol first indirect effect (Twomey, 1977), and it is denoted as a general cooling effect in terms of global radiation balance. More fundamentally, the aerosol effects on cloud reflectance result from the cloud microphysical response to aerosol concentration (e.g., aerosol-cloud interaction, ACI).

15   The magnitude and sensitivity of aerosol-cloud interactions in low-level clouds have been investigated by numerous studies, using various observational datasets such as ground-based measurements (Garrett et al., 2004; Feingold et al., 2006; Kim et al., 2008; McComiskey et al., 2009; Wang et al., 2013, 2018a), satellite retrieved products (Sekiguchi et al., 2003; Su et al., 2010) and airborne in situ measurements (Twohy et al., 2013; Painemal and Zuidema, 2013;

20   Zhao et al., 2018). However, large variations exist among various assessments, because of intrinsic instrument uncertainty, differing analysis methods, and more physically, the inherent variation in aerosol properties. The physical mechanism underlying the aerosol effect on clouds is that aerosols activate as cloud condensation nuclei (CCN) and then interact with cloud microphysical features. The efficacy of the activation of CCN has been widely known to be

25   influenced by aerosol size distribution and chemical composition which are the primary sources of uncertainty in assessing the aerosol-cloud interaction (Dusek et al., 2006; McFiggans et al., 2006; Liu and Li, 2014; Che et al., 2016).

Previous studies have suggested that the composition of aerosols can be identified by their optical properties such as aerosol optical depth, single scattering albedo, and Ångström

exponent (Clarke et al., 2004; Bergstrom et al., 2007; Clark et al., 2007; Russell et al., 2010; Cappa et al., 2016). For instance, fine mode carbonaceous particles (e.g., black and organic carbon) have strong light absorbing abilities in the ultraviolet and visible spectra (Logan et al., 2013). On the other hand, urban pollution aerosols associated with sulfate and nitrate particles

5   are considered as weakly absorbing aerosols (Eck et al., 1999, 2005; Bergstrom et al., 2007; Chin et al., 2009). Although studies have been done to classify aerosol types using the absorption Ångström exponent, which is associated with the absorptive spectral dependence of particles, this parameter has limited value when there are mixtures of different aerosol species that share similar spectral dependences (Bergstrom et al., 2007; Lack and Cappa, 2010).

10   Alternatively, the single scattering albedo (and co-albedo) can be used to better separate the aerosol types since it focuses on the relative absorbing ability of aerosols at specific wavelengths (Logan et al., 2013; Tian et al., 2017). Given the wide availability of aerosol optical property measurements, the feasibility of inferring aerosol species from their optical properties is useful particularly in areas with no direct measurements of aerosol chemical

15   composition (Logan et al., 2013; Schmeisser et al., 2017).

The Atmospheric Radiation Measurement (ARM) program initiated by the U. S. Department of Energy (DOE) aims to improve the parameterization of clouds in global climate models (Stokes and Schwartz, 1994). Thus far, the ARM program has established over 20 years of long-term ground-based point measurements of cloud properties and surface measured

20   aerosol properties at the Southern Great Plain (SGP) site which represents typical continental conditions (Ackerman and Stokes, 2003; Dong et al., 2006). The size and composition of aerosols have been found to have a considerable seasonal and regional dependence, and their impacts on clouds also vary with different aerosol regimes (Sorooshian et al., 2010; Logan et al., 2018). The prevailing fine mode aerosols at ARM-SGP site typically contain organic and

25   black carbon associated with biomass burning and inorganic aerosols composed of sulfate and nitrate species (Parworth et al., 2015; Logan et al., 2018). The differences in intrinsic hygroscopicity among those aerosol species play various roles in aerosol activation processes and consequently lead to various interactions with clouds. Thus, it is necessary to investigate the aerosol and cloud properties as well as the magnitude of the ACI index at the ARM-SGP

site, in order to (a) enhance the understanding of ACI and (b) reduce the uncertainty in quantifying the ACI and associated radiative effects when modeling aerosol influences on low level continental clouds.

In this study, the aerosol and cloud properties at the ARM-SGP site from 16 selected non-precipitating low-level stratiform cloud cases from the 2007-2012 period are examined. Details of the observational measurement platforms and methods are introduced in section 2. The development and analysis of the ACI for the 16 cases, the aerosol activation and cloud microphysical responses as well as consequent cloud radiative effects under different aerosol absorptive properties are investigated in section 3. Lastly, a summary of our findings and future work is presented in section 4.

2   Data and methods

2.1   Cloud Properties

2.1.1   Cloud Boundaries

The cloud boundaries at the ARM-SGP site were primarily determined by the ARM Active Remotely-Sensed Cloud Locations (ARSCL) product, which is a combination of data detected by multiple active remote-sensing instruments, in particular, the Millimeter-wavelength Cloud Radar (MMCR). The MMCR operates at a frequency of 35 GHz (and wavelength of 8.7 mm) with a zenith pointing beam width of 0.2° and provides a continuous time-height profile of radar reflectivity with temporal and spatial resolutions of 10 seconds and 45 m, respectively (Clothiaux et al., 2000). After 2011, the MMCR was replaced by the Ka-band ARM Zenith Radar (KAZR) which has the same operating frequency and shares similar capabilities as the MMCR, but with the major improvement of a new receiver that allows for more sensitivity in cloud detection (Widener et al., 2012). The temporal and vertical resolutions of KAZR-detected reflectivity are 4 seconds and 30 m, respectively. The cloudy condition as well as cloud top height is identified via cloud radar reflectivity.

The cloud radar is sensitive to the sixth moment of droplet size distribution and can be contaminated by insects below cloud base (Dong et al., 2006). The ceilometer and Micropulse Lidar (MPL), which are sensitive to the second moment, were calibrated with radar reflectivity

to identify an accurate cloud base estimation. Hence, the lidar-radar pair provides the most precise determination of cloud boundaries from a point-based perspective. In this study, the cloud base and top heights were averaged into 5-min bins where the low-level stratus cloud is defined as a cloud-top height lower than 3 km with no overlying cloud layer (Xi et al., 2010).

2.1.2 Cloud Microphysical Properties

The cloud liquid water path (LWP), defined as the column-integrated cloud liquid water, was retrieved based on the measured brightness temperatures from the Microwave Radiometer (MWR) at 23.8 and 31.4 GHz, using the statistical method described in Liljegren et al. (2001). The uncertainty of LWP retrieval is 20 $g\,m^{-2}$ for LWP less than 200 $g\,m^{-2}$ and around 10% for LWP higher than 200 $g\,m^{-2}$. In this study, we exclude the data points with LWPs less than 20 $g\,m^{-2}$ to eliminate optically thin clouds, as well as exclude the samples with LWPs greater than 300 $g\,m^{-2}$ to prevent potential precipitation contamination issues (Dong et al., 2008).

For microphysical properties of low-level stratus, following the methods developed by Dong et al. (1998), the daytime information of layer-mean cloud effective radius (r_e) can be parameterized by:

$$r_e = -2.07 + 2.49LWP + 10.25\gamma - 0.25\mu_0 + 20.28LWP\gamma - 3.14LWP\mu_0, \qquad (1)$$

where γ is the solar transmission, μ_0 is the cosine of solar zenith angle, and the units of r_e and LWP are μm and 100 $g\,m^{-2}$, respectively. N_d is obtained after r_e is known, by the following calculation:

$$N_d = \left(\frac{3LWP}{4\pi\rho_w r_e^3 \Delta Z}\right)\exp(3\sigma_x^2), \qquad (2)$$

where N_d has units of cm^{-3}, ΔZ is cloud thickness determined from cloud boundaries with units of m, and σ_x is the width of lognormal size distribution of cloud droplet, which is assumed to be a constant value of 0.38 (Miles et al., 2002). The algorithms have been evaluated using aircraft in situ measurements over the ARM-SGP site (Dong et al., 2002, 2003), with an uncertainty for retrieved daytime r_e of 10% and N_d of 20-30%, with respect to the 5-min averaged data.

2.2 Aerosol Properties

Surface aerosol properties were collected from the Aerosol Observation System (AOS), a platform consisting of an array of instruments to monitor real time aerosol information. The total condensation nuclei number concentration (N_a) represents the overall loading of aerosol particles with diameter larger than 10 nm and was obtained by the TSI model 3010

5   condensation particle counter. The aerosol scattering coefficient (σ_{sp}) was measured by the TSI model 3653 nephelometer at three wavelengths: 450, 500, and 700 nm. The relative humidity inside the nephelometer was set to 40% to maintain a dry condition and prevent potential aerosol hygroscopic effects (Jefferson, 2011), and the quality of retrievals has been assured using the Anderson and Ogren (1998) method. The absorption coefficient (σ_{ap}) was measured

10   by the Radiance Research particle soot absorption photometer (PSAP) at three slightly different wavelengths (470, 528 and 660 nm), with the calibration and quality control process done by the method developed in Anderson et al. (1999). Note that both the nephelometer and PSAP employ two impactors with size cuts of 1 μm and 10 μm. The measurements switch between total aerosol (<10 μm) and submicron aerosol (<1 μm) every hour. In this study, the

15   submicron aerosol optical properties were interpolated into 5-min averages to match the cloud microphysical properties.

The optical particle counter developed by Droplet Measurement Technologies is used to measure the CCN number concentration (N_{CCN}). The supersaturation (SS) level inside the instrument cycles between 0.15% and 1.15% every hour. The CCN activity can be presented

20   as a function of SS: $N_{CCN} = cSS^k$ (Twomey, 1959), where c and k are calculated by using a power law fit for each hour. In this study, 0.2% is used as this represents typical supersaturation conditions of low-level stratus clouds (Hudson and Noble, 2013; Logan et al., 2014; Logan et al., 2018).

2.3   Boundary Layer Condition

25   Given the fact that the aerosol properties were measured at the surface, there is a question of how to link surface aerosols to what actually happens in clouds aloft. This study adopts the method presented in Dong et al. (2015), which defined the boundary layer condition into two categories: coupled and decoupled. The vertical sounding profiles at a 1-min temporal

resolution were collected from the ARM Merged Sounding product with a vertical resolution of 20 m below 3 km (Mace et al., 2006; Troyan, 2012). The vertical profiles of liquid water potential temperature (θ_L) and total water mixing ratio (q_t) for coupled and decoupled boundary layer conditions, as well as the criteria to differentiate between them, are illustrated in Fig. 1. The coupled condition was identified by the change of θ_L and q_t from surface layer to cloud base of less than 0.5 K and 0.5 g/kg, respectively. In that case, the boundary layer is considered to be well-mixed and suggests that the surface aerosols are comparable to in-cloud aerosols. However, the θ_L and q_t vary more drastically from surface to cloud base under decoupled conditions, which denotes a stratification of the sub-cloud layer thereby disconnecting the surface aerosols from the ones aloft. Therefore, selecting cloud cases under coupled conditions can better constrain the thermodynamic condition since the measured surface aerosols are representative in terms of aerosol-cloud interaction.

2.4 Shortwave radiation fluxes at the Surface

The surface measured broadband downwelling shortwave (SW) radiation fluxes and estimated clear-sky SW fluxes were collected from Radiative Flux Analysis Value Added Products (Long and Ackerman, 2000; Long and Turner, 2008), with an uncertainty of $10\ \mathrm{W\ m^{-2}}$. The combination of cloudy and clear-sky SW fluxes was used to calculate the cloud radiative effect. In order to minimize the influence of non-cloud factors, such as solar zenith angle and surface albedo, a representation of relative cloud radiative effect (rCRE) is defined as

$$\mathrm{rCRE} = 1 - \mathrm{SW}_{\mathrm{cld}}^{dn}/\mathrm{SW}_{\mathrm{clr}}^{\mathrm{dn}}, \tag{3}$$

where $\mathrm{SW}_{\mathrm{cld}}^{dn}$ and $\mathrm{SW}_{\mathrm{clr}}^{\mathrm{dn}}$ are cloudy and clear-sky downwelling shortwave radiation fluxes, respectively (Betts and Viterbo, 2005; Vavrus, 2006; Liu et al., 2011).

2.5 Selection of low-level stratus cloud cases

As previously discussed, the selection of cloud cases is limited by the following criteria: non-precipitating and cloud-top height less than 3 km with lifetime more than 3 hours under coupled boundary layer conditions. Only daytime cloudy periods were considered, as suggested by Feingold et al. (2003). The 16 cases were selected during the 6-year period from 2007 to

2012 and a detailed time period of each case is listed in Table 1. Most cases occurred during the winter and spring months since low-level cloud occurrences are higher during those seasons (Dong et al., 2006). The 72-hour NOAA HYSPLIT backward trajectories (Stein et al., 2015) for sub-cloud air parcels that advected over the ARM-SGP site are used to identify the aerosol

5   source regions (Logan et al., 2018). Aerosol plumes consisting of different species from local sources and long-range transport can impact the ARM SGP site because of different transport pathways and can induce different cloud responses which are further investigated in this study.

3   Result and Discussion

3.1   Aerosol and cloud properties of selected cases

10   The probability density functions (PDFs) of aerosol and cloud properties from all 16 cases are shown in Fig. 2. For the aerosol properties shown in top panel, the Ångström Exponent (AE) was calculated based on nephelometer observed spectral scattering coefficient (σ_{sp}) at 450 nm and 700 nm, using the equation of $AE_{450-700nm} = -\log(\sigma_{sp450}/\sigma_{sp700})/\log(450/700)$. The negative log-log slope denotes the relative wavelength dependence of particle

15   optical properties due to differences in particle sizes (Schuster et al., 2006). Therefore, AE can be a good indicator of aerosol particle sizes since AE > 1 indicates the particle size distributions dominated by find mode aerosols (submicron), while AE < 1 denotes the dominance of coarse mode aerosols (Gobbi et al., 2007; Logan et al., 2010). The aerosol Fine Mode Fraction (FMF) is given by the ratio, $\sigma_{sp1}/\sigma_{sp10}$, where σ_{sp1} and σ_{sp10} are the nephelometer measured

20   scattering coefficients at 550 nm for fine mode aerosols (1 μm size cut) and total aerosols (10 μm size cut), respectively. This ratio indicates the dominant influence of fine mode aerosols owing to the physical properties of the entire aerosol plume. For example, FMF values greater than 0.6 represent the dominance of fine mode aerosols, and values that less than 0.2 represent coarse mode aerosols (Anderson et al., 2003). As illustrated in Fig. 2b and 2c, the

25   fine mode aerosols are dominated from the 16 selected cases with the evidences where all AE values are higher than 1, most of the values ranged from 1.5 to 2 and most of the FMF values are greater than 0.6, the majority range from 0.7 to 0.9.

The results from the distributions of AE and FMF indicate the major dominance of fine mode aerosols in the aerosol plumes from the 16 selected cases. However, the variation in aerosol single scattering albedo (SSA) suggests different roles of the aerosol absorptive properties that influence total light extinction which in turn result from different aerosol species in the plume. This is further explained in section 3.3. The distributions of N_a, N_{CCN}, and N_d show typical continental aerosol conditions with mean values of 1050 cm^{-3}, 475 cm^{-3}, and 297 cm^{-3}, respectively, and r_e are more normally distributed with the majority of values between 7-9 μm. Note that the variation in the PDF of LWP is relatively small which allow for a better investigation of the LWP dependence of cloud microphysical properties.

3.2 Measured Aerosol-Cloud-Interaction

To examine the microphysical response of cloud to aerosol loading, the quantitative Aerosol-Cloud-Interaction (ACI) term can be expressed as

$$ACI_r = -\frac{\partial \ln(r_e)}{\partial \ln(\alpha)}\Big|_{LWP}, \tag{4}$$

where α denotes aerosol loading. ACI_r represents the relative change of layer mean r_e with respect to the relative change of aerosol loading thereby emphasizing the sensitivity of the cloud microphysical response (Feingold et al., 2003; Garrett et al., 2004). Note that values of ACI_r have boundaries of 0-0.33, where the lower bound means no change of cloud microphysical properties with aerosol loading and the upper bound indicates a linear relationship.

As suggested by previous studies, the ACI_r should be calculated and compared at constant LWP owing to the dependence of r_e on LWP (Twomey et al, 1977; Feingold et al., 2003). Therefore, in this study we use six LWP bins ranging from 0-300 $g\,m^{-2}$ with bin size of 50 $g\,m^{-2}$ and then group the sample data accordingly. Note that the first bin is actually 20-50 $g\,m^{-2}$ due to the elimination of LWP less than 20 $g\,m^{-2}$. The r_e-N_{CCN} relationship is presented in Fig. 3a where only the samples from three LWP bins are used to illustrate the r_e-N_{CCN} response. In general, r_e decreases with increasing CCN number concentration as expected. The ACI_r values from six LWP bins show a generally decreasing trend of ACI_r with increasing LWP (Fig. 3b). Particularly, this decreasing trend is more obvious in a range of LWPs that are less than 150 $g\,m^{-2}$. The higher values of ACI_r at lower LWP indicate that the clouds are more

susceptible to aerosol loading under lower liquid water availability. When LWP increases, there is increased collision-coalescence activity within the cloud which results in the reduction of N_d as shown in Fig. 3b (blue diamonds). This partly leads to the damping of cloud microphysical sensitivity as evidenced by decreased ACI_r (Kim et al., 2008; McComiskey et al., 2009). The

5 observed range of ACI_r values (0.09–0.24) and mean value of 0.145 ± 0.05 are both consistent with previous studies investigating ACI_r using ground-based measurements. At the ARM SGP site, Kim et al. (2008) found similar decreasing microphysical activity with higher LWP in ACI_r values ranging from 0.04 to 0.17 from a three-year study (1999-2001). Feingold et al. (2003) found ACI_r values of 0.02 to 0.16 from an intensive operation period during May

10 2003, while Sena et al. (2016) reported values ranging from 0.19-0.37 from a case study in 2006. At other regions, McComiskey et al. (2009) measured ACI_r values in the range of 0.05-0.16 with similar microphysical behavior for marine stratus clouds, and Garrett et al. (2004) found ACI_r with a range of 0.13-0.19 in the Arctic regions. The assumption when using ACI_r is that there exists a significant relationship between aerosol loading and CCN, thus a nearly

15 constant fraction of aerosol effectively activates as CCN. In essence, aerosol loading is more important than the aerosol size and composition. However, the ACI_r values from all samples should be interpreted with caution since this assumption may not always be valid and is conditional. In order to further examine the role of aerosol species in ACI_r, the samples from the 16 selected cases are divided into two groups according to their absorptive regime which is

20 discussed in the following section.

3.3 Relationship between aerosol absorptive properties and ACI

3.3.1 Aerosol absorptive properties of the 16 selected cases

The measured absorptive properties of aerosols can aid in inferring the general information of different aerosol species since different types of aerosols can demonstrate

25 different absorptive behaviors at certain wavelengths. Aerosol plumes dominated by organic carbonaceous particles tend to represent strong absorptive capabilities in the visible spectrum but weakly absorb in near infrared (Dubovik et al., 2002; Lewis et al., 2008) while black carbon particles (e.g., soot) absorb across the entire solar spectrum with a weak dependence on wavelength (Schuster et al., 2005; Lack and Cappa, 2010). However, when the aerosol plume

is dominated by anthropogenic inorganic pollution, the absorbing ability becomes even weaker (Clark et al., 2007), partly due to sulfate chemical species (Chin et al., 2009). Therefore, the general existence of carbonaceous and pollution particles can be inferred via absorptive properties.

5   In this study, we adopt the classification method involving AE and the ratio of aerosol absorption coefficient to total extinction coefficient or single scattering co-albedo, ($\omega_{abs} = \sigma_{abs}/(\sigma_{abs} + \sigma_{scat})$), defined in Logan et al. (2013). This parameter represents the contribution of aerosol light absorbing (rather than scattering) capabilities to aerosol light extinction which gives more information about aerosol composition (Logan et al., 2013). The ω_{abs} at a

10   wavelength of 450 nm along with the $AE_{450-700nm}$ of all the samples are shown in Fig. 4. A ω_{abs} value of 0.07 is used as a demarcation line of aerosols that are weakly and strongly absorbing. This value was determined using a frequency analysis performed at four AERONET sites that are dominated by single aerosol modes (Logan et al., 2013). Of the 16 cases, six cases are dominated by strongly absorbing aerosols, seven cases are dominated by weakly absorbing

15   aerosols, and three cases have samples which broadly scatter across the ω_{abs} domain which denotes a mixture of different absorbing aerosol species. It is interesting to note that the majority of the winter cases are dominated by weakly absorbing aerosols while most of the spring cases exhibit a strongly absorbing aerosol dominance which suggests that the aerosol plumes over the SGP site also have a seasonal dependence. This will be worth further

20   investigation when more sufficient aerosol observations at the SGP site become available.

3.3.2   Aerosol and cloud properties under different absorptive regimes

Figures 5a-5c show the PDFs of total N_a, N_{CCN}, and AE for the two absorptive regimes. Both distributions and mean values of N_a, however, the mean N_{CCN} for the weakly absorptive regime (524 cm^{-3}) is larger than the strongly absorptive regime (411 cm^{-3}) with more higher

25   values above 1000 cm^{-3}. This suggests different responses of CCN concentration to aerosols that have similar magnitudes but different absorptive properties. The AE distributions suggest dominant fine mode aerosol contributions for both regimes. As for the cloud microphysical property distributions, cloud samples between the two regimes exhibit different characteristics (Fig. 5d-5f). Cloud LWPs and r_e values under the strongly absorptive regime have larger values

Atmospheric
Chemistry
and Physics
Discussions

Open Access

EGU

which contrasts with those under the weakly absorptive regime. On the other hand, cloud droplets under the weakly absorptive regime have a distribution of N_d that is positively skewed with majority (76%) of values below 300 cm^{-3}. On average, the weakly absorbing regime has higher cloud droplet number concentrations and smaller cloud droplet effective radii (355

5 cm^{-3} and 6.9 μm, respectively) compared to the strongly absorbing regime (221 cm^{-3} and 8.3 μm). Note that the LWP under the strongly absorptive regime is generally higher. Thus, the question behind these results is whether the differences in cloud microphysical properties between the two regimes are due to the difference in LWP. As previously stated by Dong et al. (2015), cloud droplets generally grow larger at higher LWP which eventually leads to lower

10 droplet number concentration.

3.3.3 Relationship of aerosol activating as CCN under different absorptive regimes

The measured N_a and N_{CCN} under the strongly and weakly absorbing aerosol regimes are plotted in Fig. 6. Note that N_a samples from the strong and weak regimes cover a broad range of values from 200-3500 cm^{-3} suggesting a wide variety of aerosol loading conditions. These

15 highly overlapping distributions allow quantitative comparison between the ratios of N_{CCN} to N_a. For a broad range of N_a, especially 200-700 cm^{-3} and 1200-3500 cm^{-3}, the majority of sample points from the strongly absorbing regime are located below the samples of the weakly absorbing regime. The linear regressions between N_{CCN} and N_a for two regimes demonstrate the sensitivity of $CCN_{0.2\%SS}$ to total aerosol loading. With the slopes of both regressions pass

20 the significant test at 95% confidence level, note that the slope derived from weak regime is slightly steeper than the one derived from strong regime, indicating that the N_{CCN} values in weakly absorptive regime increase faster than those in strongly absorptive regime with same amount of aerosol increment. On average, 54% of weakly absorbing aerosols can effectively activate as CCN compared to 45% of the strongly absorbing aerosols.

25 The aerosol capacity to activate as CCN is substantially associated with size and chemical composition (Seinfeld and Pandis, 2006). Although it is generally considered that the role of aerosol particle size distribution is more important than the chemical component in terms of becoming CCN (Dusek et al., 2006), many studies have found that aerosol chemical composition can also have a non-negligible impact on the aerosol activating ability under

different polluted conditions (Rose et al., 2011; Che et al., 2016), especially under low supersaturation conditions. According to Kohler theory, the critical level of supersaturation for aerosol activation depends on the aerosol solubility which decreases with increasing soluble particle number concentration. Hence, the role of aerosol chemical composition is more

5   important at lower supersaturation and diminishes with increasing supersaturation level (Zhang et al., 2012).

As discussed in section 3.3.1, the weakly absorptive and strongly absorptive regimes are linked to aerosol plumes that are dominated by pollution and carbonaceous aerosols, respectively. Therefore, the difference in the ability of aerosol activation between the two

10   regimes can be explained by the different hygroscopicity factors of the particle types. For example, anthropogenic pollution is associated with inorganic particles that are highly hygroscopic and have great ability in taking up water (Hersey et al., 2009; Massling et al., 2009; Liu et al., 2014), while carbonaceous species (e.g., black and organic carbon) exhibit varying degrees of hygroscopicity with species dominated by hydrophobic soot and black carbon being

15   the least hygroscopic (Shinozuka et al., 2009; Rose et al., 2010). Thus, for given amount of aerosol loading, aerosols in the weakly absorptive regime can better attract water and result in more aerosol particles to be activated as CCN.

Due to the lack of detailed chemical observations for all the cloud sample periods, as well as the uncertainties among aerosol optical and microphysical properties induced by aerosol

20   transformation processes such as aging and mixing (Wang et al., 2018b), the bulk activation rates revealed from this study cannot be significantly distinguished from each other. However, the effect of different aerosol species inferred by the absorptive properties with respect to aerosol activation are evident, especially at the 0.2% supersaturation level.

3.3.4   LWP dependence of aerosol and CCN activation under different absorptive regime

25   In order to better understand the role of aerosol activation ability in the microphysical process from aerosol to CCN and then to cloud droplet, comparisons must be considered under similar available moisture conditions due to the discrepancy of LWP between the two regimes. Accordingly, the sorted N_a values by stratified LWP are presented in Fig. 7a, along with the conversion ratios of N_{CCN}/N_a which are denoted by solid lines. For LWP ranging from 0-300

Atmospheric
Chemistry
and Physics
Discussions
Open Access
EGU

g m^{-2}, the ratios of N_{CCN}/N_a under both regimes increase slightly with increased LWP. In addition, all the values of N_{CCN}/N_a from the weakly absorptive regime (ranging from 0.4 to 0.6) are higher than those from the strongly absorptive regime (ranging from 0.3 to 0.5).

Taking the variation of N_{CCN} into account, the conversion rates of N_{CCN} to N_a under low

5   LWP conditions (<50 g m^{-2}) in both absorptive regimes could be simply due to the linear combination of high aerosol concentration and insufficient moisture supply such that aerosols are competing against each other thus resulting in a low conversion rate. However, as the LWP increases, the activation rates tend to increase as well, especially at LWP values higher than 100 g m^{-2}. In fact, the values of N_a for both regimes are relatively small with little variation

10   for LWP > 100 g m^{-2}, while the N_{CCN}/N_a ratio demonstrates a more noticeable increasing trend in the weakly absorptive regime. Despite the higher aerosol loading in the strongly absorptive regime at higher LWPs, there are still more weakly absorbing aerosols being activated, which corresponds to greater water uptake ability.

As for the process from CCN to cloud droplet, a similar assessment is presented in Fig.

15   7b, which illustrates the N_{CCN} values and conversion rates of N_d to N_{CCN} in relation to LWP. The conversion rates of N_d/N_{CCN} for the weakly absorptive regime range from 0.45 to 0.9 with a mean value of 0.68, and highly fluctuates with LWP. In contrast, the rates for the strongly absorptive regime show lower values and less variability (from 0.45 to 0.6) with a mean value of 0.54. It is interesting to note that the variation of N_d/N_{CCN} for the strongly absorptive regime

20   mimics the variation in N_{CCN} with LWP, indicating a relatively lower aerosol to CCN activating capacity. Therefore, the conversion rate for CCN to cloud droplet shows no significant dependence on LWP, which is consistent with previous research that suggests the response of N_d to the change in N_{CCN} has no fundamental relationship with LWP (McComiskey et al., 2009).

The overall differences in CCN conversion ratio are likely a result of the differences in

25   water uptake abilities as previously discussed. Alternatively, it can possibly be related to cloud base vertical velocity as the sensitivity of cloud droplet to aerosol loading is enhanced with increasing column maximum updraft speed (Feingold et al., 2003), which is not included in this study due to lack of observations from the ground-based Doppler lidar. Moreover, it is noteworthy that the uncertainty in deriving the CCN activation rate can be deduced by the

uncertainty in N_d retrieval, since the retrieval method assumes a constant lognormal width for cloud droplet size distribution while in nature those widths are variable.

3.3.5   LWP dependence of re and Nd under different absorptive regimes

In the previous section, we examined the activation rates of aerosol to CCN and then from

5   CCN to cloud droplet between the two regimes as well as their dependences on LWP, that eventually led to the cloud droplet variation for a given LWP range. Figures 7c-7d demonstrate that r_e increases while N_d decreases with increased LWP up to roughly 150 g m^{-2} in both regimes. Note that as the LWP increases to values beyond 150 g m^{-2}, N_d values in both regimes show less variation with LWP while r_e values in the strongly absorptive regime also show little

10   variation which implies limited growth even with increasing water availability. However, the r_e values in the weakly absorptive regime range from 7.3 to 8.8 μm, which suggests that under a given number concentration, the cloud droplet can grow by continuing to collect moisture. As shown in each LWP bin, the r_e values in the weakly absorptive regime are smaller than those in the strongly absorptive regime, while the N_d values in the strongly absorptive regime are

15   smaller than those in the weakly absorptive regime. For a given LWP, a greater number of CCN in the weakly absorptive regime can be converted to cloud droplets because of greater water uptake ability, resulting in higher number concentrations of smaller cloud droplets, while the lower CCN activating capacity in the strongly absorptive regime led to fewer and larger cloud droplets at fixed LWP. The different behavior of r_e with respect to the variation in LWP indicates

20   that cloud droplets that form from weakly absorbing aerosols have greater growth ability which further supports the previous discussion about the water uptake ability of these aerosols, in particular.

3.3.6   Aerosol-cloud-interaction under different absorptive regimes

To examine the sensitivity of clouds to both weakly and strongly absorbing aerosol

25   loading, the relationship between cloud r_e and aerosol absorption are shown in Fig. 10. Two LWP ranges (0-50 g m^{-2} and 200-250 g m^{-2}) are selected in order to better represent ACI$_r$ at low and high LWP conditions. For the examination of r_e as a function of N_a (Fig. 8a and 8b) and N_{CCN} (Fig. 8c and 8d), the values of ACI$_r$ in the weakly absorptive regime are higher than those in the strongly absorptive regime. This suggests that the cloud droplets are more sensitive

to weakly absorbing aerosols than to strongly absorbing aerosols. In other words, if there is some increment in aerosol particles, clouds influenced by weakly absorbing aerosols will respond to this increment more effectively and decrease faster in droplet sizes relatively. Under high LWP conditions, the values of measured ACI_r are lower and show less difference between

5   the two regimes, which is in agreement with previous discussions on the sensitivity of cloud microphysical properties to aerosol loading.

Note that in general when N_{CCN} is used to represent aerosol concentration, the derived ACI_r values are larger than the ACI_r represented by N_a, which indicates clouds are more sensitive to CCN than solely aerosol particles. One explanation is that when we link the cloud

10   droplets together with aerosol properties such as number concentration or scattering coefficient to assess their relationship, the implicit assumption is that the aerosol particles undergo a specific nucleating process in which a constant fraction of them can be treated effectively as cloud droplets (Kim et al., 2008). In nature, the activation rates are not constant and indeed vary with aerosol species and ambient water availability. Therefore, by considering the one-

15   step process from CCN to cloud droplet, the assessment of ACI_r via N_{CCN} can reveal the interaction between aerosol and cloud more accurately.

3.4   Cloud shortwave radiative effects under different absorptive regimes

Aerosols with different absorptive properties can alter the ability of clouds to reflect incoming shortwave radiation. Accordingly, cloud radiative effects on shortwave radiation for

20   the two absorptive regimes are investigated. Both cloudy and clear-sky downwelling shortwave fluxes for samples in the weakly absorptive regimes are generally higher than those in the strongly absorptive regime (not shown in here), largely owing to the discrepancies in solar zenith angle, seasonal variation of insolation, and surface albedo. Therefore, to ensure the comparison is under minimum influence of non-cloud factors, the shortwave relative Cloud

25   Radiative Effects (rCREs) are introduced and their dependency on LWP between the two regimes are examined. With all else being equal, as shown in Fig. 9, rCREs in both regimes noticeably increase when the LWP is less than $150 \, \mathrm{g \, m^{-2}}$. Under fixed LWP, rCREs in the weakly absorptive regime are always higher than those in strongly absorptive regime, because the greater activating ability of the weakly absorbing aerosols leads to higher N_d and smaller r_e

as opposed to the strongly absorbing aerosols. Thus, clouds with a higher amount of small cloud droplets contribute more to the extinction of incident solar radiation. The difference between mean rCRE for the weakly absorptive and strongly absorptive regimes is small but non-negligible (~0.05). Quantitatively speaking, taking the climatological downwelling solar

5   flux of the winter season (~ 150 W m^{-2}, Dong et al., 2006) as an example, the extinction of incident solar radiation by clouds that develop from weakly absorbing aerosols is 7.5 W m^{-2} more than those by clouds from strongly absorbing aerosols. From independent radiative measurements, the phenomenon that clouds are more susceptible to weakly absorbing aerosols is further evidenced.

10   **4   Conclusions**

A total of 16 non-precipitating overcast low-level stratiform cloud cases under daytime coupled boundary layer conditions were selected in order to investigate the sensitivity of cloud microphysical properties to aerosol physicochemical properties. The Ångström exponent and fine mode fraction distributions indicate that the aerosol plumes that advected to the SGP site

15   during all the selected cases were dominated by fine mode particles, while the variation in aerosol single scattering albedo suggests different characteristics of optical properties among the aerosol plumes. In terms of the sensitivity of cloud droplets to aerosol number concentration, the values of ACI$_r$ range from 0.09 to 0.24 with the mean of 0.145 $\pm$ 0.05, which supports the finding of previous studies using ground-based measurements. The magnitude of ACI$_r$ shows

20   a decreasing trend with increasing LWP, partly owing to the enhanced collision-coalescence process accompanied by higher LWP. However, clouds that develop under lower LWP conditions are more susceptible to aerosol loading, owing to the enhanced competition between aerosols to activate as cloud droplets with a limited supply of moisture.

The analysis of the N$_{CCN}$/Na ratio under the two regimes further demonstrates that weakly

25   absorbing aerosols have statistically significant higher activation rates (mean ratio of 0.54) than the strongly absorbing aerosols (mean ratio of 0.45). The fraction of weakly absorbing aerosols that activate as CCN show a noticeable increase with increased LWP, while the activation rates for strongly absorbing aerosols tend to slightly increase with LWP under comparable aerosol loading conditions. This is likely related to the hygroscopicity associated with the aerosol

17

species. For example, weakly absorbing aerosols are typically dominated by pollution aerosols that have greater water uptake ability, while strongly absorbing aerosols are generally hydrophobic, such as freshly emitted black and organic carbon (Wang et al., 2018b).

Consequently, the conversion rates of N_d/N_{CCN} for weakly absorbing aerosols are higher than the strongly absorbing aerosols. As a result, cloud droplets that form from weakly absorbing aerosols tend to have smaller sizes and higher concentrations than cloud droplets forming from strongly absorbing aerosols. Furthermore, the cloud droplets under the weakly absorptive regime exhibit a greater growing ability, as given by larger r_e values that increase with LWP under similar N_d.

Under low LWP conditions (<100 g m^{-2}), the measured ACI_r under the weakly absorptive regime is relatively higher, indicating clouds have greater microphysical responses to weakly absorbing aerosols than strongly absorbing aerosols. Also, the observed ACI_r with respect to N_{CCN} is generally higher than N_a, which demonstrates that the mechanism from CCN to cloud droplet is more straightforward than from aerosol particle to cloud droplet. Under higher LWP conditions, the damping of ACI_r is more evident, which is consistent with the results from all the cases. As a result, clouds that develop from weakly absorbing aerosols serving as CCN exhibit a stronger shortwave cloud radiative influence than clouds originating from strongly absorbing aerosols. Additional future work will focus on investigating the seasonal dependence of aerosol sources, with respect to their physicochemical properties. The aerosol-cloud-interaction processes under the influence of different aerosol types associated with airmasses and the sensitivity to dynamic and thermodynamic factors over the will be further examined.

Author contributions. The original idea of this study has discussed by XZ, BX, and XD. XZ performed the analyses and wrote the manuscript. XD, TL, YW, and PW participated in further scientific discussion and provided substantial comments and edits on the paper.

Competing interests. The authors declare that they have no conflict of interest.

References

Ackerman, T. P. and Stokes, G. M.: The atmospheric radiation measurement program, Phys. Today, 56(1), 38–44, doi:10.1063/1.1554135, 2003.

10   Anderson, T. L. and Ogren, J. A.: Determining Aerosol Radiative Properties Using the TSI 3563 Integrating Nephelometer, Aerosol Sci. Technol., 29(1), 57–69, doi:10.1080/02786829808965551, 1998.

Anderson, T. L., Covert, D. S., Wheeler, J. D., Harris, J. M., Perry, K. D., Trost, B. E., Jaffe, D. J., and Ogren, J. A.: Aerosol backscatter fraction and single scattering albedo: Measured

15   values and uncertainties at a coastal station in the Pacific Northwest, J. Geophys. Res., 104, 1999.

Anderson, T. L., Masonis, S. J., Covert, D. S., Ahlquist, N. C., Howell, S. G., Clarke, A. D., and McNaughton, C. S.: Variability of aerosol optical properties derived from in situ aircraft measurements during ACE-Asia, J. Geophys. Res., 108(D23), ACE 15-1-ACE 15-

20   19, doi:10.1029/2002jd003247, 2003.

Betts, A. K. and Viterbo, P.: Land-surface, boundary layer, and cloud-field coupling over the southwestern Amazon in ERA-40, J. Geophys. Res. D Atmos., doi:10.1029/2004JD005702, 2005.

Cappa, C. D., Kolesar, K. R., Zhang, X., Atkinson, D. B., Pekour, M. S., Zaveri, R. A., Zelenyuk,

25   A., and Zhang, Q.: Understanding the optical properties of ambient sub- and supermicron particulate matter: results from the CARES 2010 field study in northern California, Atmos. Chem. Phys., 16, 6511-6535, https://doi.org/10.5194/acp-16-6511-2016, 2016.

Cazorla, A., Bahadur, R., Suski, K. J., Cahill, J. F., Chand, D., Schmid, B., Ramanathan, V., and Prather, K. A.: Relating aerosol absorption due to soot, organic carbon, and dust to

emission sources determined from in-situ chemical measurements, Atmos. Chem. Phys., 13, 9337-9350, https://doi.org/10.5194/acp-13-9337-2013, 2013.

Che, H. C., Zhang, X. Y., Wang, Y. Q., Zhang, L., Shen, X. J., Zhang, Y. M., Ma, Q. L., Sun, J. Y., Zhang, Y. W. and Wang, T. T.: Characterization and parameterization of aerosol cloud condensation nuclei activation under different pollution conditions, Sci. Rep., 6(April), 1–14, doi:10.1038/srep24497, 2016.

Chin, M., Diehl, T., Dubovik, O., Eck, T. F., Holben, B. N., Sinyuk, A. and Streets, D. G.: Light absorption by pollution, dust, and biomass burning aerosols: A global model study and evaluation with AERONET measurements, Ann. Geophys., doi:10.5194/angeo-27-3439-2009, 2009.

Clarke, A. D., Shinozuka, Y., Kapustin, V. N., Howell, S., Huebert, B., Doherty, S., Anderson, T., Covert, D., Anderson, J., Hua, X., Moore, K. G., McNaughton, C., Carmichael, G. and Weber, R.: Size distributions and mixtures of dust and black carbon aerosol in Asian outflow: Physiochemistry and optical properties, J. Geophys. Res. D Atmos., doi:10.1029/2003JD004378, 2004.

Clarke, A., McNaughton, C., Kapustin, V., Shinozuka, Y., Howell, S., Dibb, J., Zhou, J., Anderson, B. E., Brekhovskikh, V., Turner, H. and Pinkerton, M.: Biomass burning and pollution aerosol over North America: Organic components and their influence on spectral optical properties and humidification response, J. Geophys. Res. Atmos., doi:10.1029/2006JD007777, 2007.

Clothiaux, E. E., Ackerman, T. P., Mace, G. G., Moran, K. P., Marchand, R. T., Miller, M. A. and Martner, B. E.: Objective Determination of Cloud Heights and Radar Reflectivities Using a Combination of Active Remote Sensors at the ARM CART Sites, J. Appl. Meteorol., doi:10.1175/1520-0450(2000)039<0645:odocha>2.0.co;2, 2007.

Dong, X., Ackerman, T. P. and Clothiaux, E. E.: Parameterizations of the microphysical and shortwave radiative properties of boundary layer stratus from ground-based measurements, J. Geophys. Res. Atmos., doi:10.1029/1998JD200047, 1998.

Dong, X., Mace, G. G., Minnis, P., Smith, W. L., Poellot, M., Marchand, R. T. and Rapp, A. D.: Comparison of Stratus Cloud Properties Deduced from Surface, GOES, and Aircraft Data

during the March 2000 ARM Cloud IOP, J. Atmos. Sci., doi:10.1175/1520-0469(2002)059<3265:coscpd>2.0.co;2, 2002.

Dong, X. and Mace, G. G.: Profiles of low-level stratus cloud microphysics deduced from ground-based measurements, J. Atmos. Ocean. Technol., doi:10.1175/1520-0426(2003)020<0042:POLLSC>2.0.CO;2, 2003.

Dong, X. Q., Minnis, P. and Xi, B. K.: A climatology of midlatitude continental clouds from the ARM SGP Central Facility: Part I: Low-level cloud macrophysical, microphysical, and radiative properties, J. Clim., doi:Doi 10.1175/Jcli3342.1, 2005.

Dong, X., Xi, B. and Minnis, P.: A climatology of midlatitude continental clouds from the ARM SGP Central Facility. Part II: Cloud fraction and surface radiative forcing, J. Clim., doi:10.1175/JCLI3710.1, 2006.

Dong, X., Minnis, P., Xi, B., Sun-Mack, S. and Chen, Y.: Comparison of CERES-MODIS stratus cloud properties with ground-based measurements at the DOE ARM Southern Great Plains site, J. Geophys. Res. Atmos., doi:10.1029/2007JD008438, 2008.

Dong, X., Schwantes, A. C., Xi, B. and Wu, P.: Investigation of the marine boundary layer cloud and CCN properties under coupled and decoupled conditions over the azores, J. Geophys. Res., doi:10.1002/2014JD022939, 2015.

Dubovik, O., Holben, B., Eck, T. F., Smirnov, A., Kaufman, Y. J., King, M. D., Tanré, D. and Slutsker, I.: Variability of Absorption and Optical Properties of Key Aerosol Types Observed in Worldwide Locations, J. Atmos. Sci., doi:10.1175/1520-0469(2002)059<0590:VOAAOP>2.0.CO;2, 2002.

Dusek, U., Frank, G. P., Hildebrandt, L., Curtius, J., Schneider, J., Walter, S., Chand, D., Drewnick, F., Hings, S., Jung, D., Borrmann, S. and Andreae, M. O.: Size matters more than chemistry for cloud-nucleating ability of aerosol particles, Science (80-.)., doi:10.1126/science.1125261, 2006.

Feingold, G., Eberhard, W. L., Veron, D. E. and Previdi, M.: First measurements of the Twomey indirect effect using ground-based remote sensors, Geophys. Res. Lett., doi:10.1029/2002GL016633, 2003.

Atmospheric
Chemistry
and Physics
Discussions

Feingold, G., Furrer, R., Pilewskie, P., Remer, L. A., Min, Q. and Jonsson, H.: Aerosol indirect effect studies at Southern Great Plains during the May 2003 Intensive Operations Period, J. Geophys. Res. Atmos., doi:10.1029/2004JD005648, 2006.

Garrett, T. J., Zhao, C., Dong, X., Mace, G. G. and Hobbs, P. V.: Effects of varying aerosol regimes on low-level Arctic stratus, Geophys. Res. Lett., doi:10.1029/2004GL019928, 2004.

Gobbi, G. P., Kaufman, Y. J., Koren, I., and Eck, T. F.: Classification of aerosol properties derived from AERONET direct sun data, Atmos. Chem. Phys., 7, 453-458, https://doi.org/10.5194/acp-7-453-2007, 2007.

Hudson, J. G. and Noble, S.: CCN and Vertical Velocity Influences on Droplet Concentrations and Supersaturations in Clean and Polluted Stratus Clouds, J. Atmos. Sci., doi:10.1175/jas-d-13-086.1, 2013.

IPCC, Climate Change 2013: The Physical Science Basis. Contribution of Working Group I to the Fifth Assessment Report of the Intergovernmental Panel on Climate Change [Stocker, T.F., D. Qin, G.-K. Plattner, M. Tignor, S.K. Allen, J. Boschung, A. Nauels, Y. Xia, V. Bex and P.M. Midgley (eds.)]. Cambridge University Press, Cambridge, United Kingdom and New York, NY, USA, 1535 pp, doi:10.1017/CBO9781107415324, 2013.

Jefferson, A.: Aerosol observing system (AOS) handbook, ARMTR-014, US Dep. of Energy, Washington, D. C., 2011.

Kim, B. G., Miller, M. A., Schwartz, S. E., Liu, Y., and Min, Q.: The role of adiabaticity in the aerosol first indirect effect, J. Geophys. Res., 113, D05210, doi:10.1029/2007JD008961, 2008.

Lack, D. A. and Cappa, C. D.: Impact of brown and clear carbon on light absorption enhancement, single scatter albedo and absorption wavelength dependence of black carbon, Atmos. Chem. Phys., 10, 4207-4220, https://doi.org/10.5194/acp-10-4207-2010, 2010.

Lewis, K., Arnott, W. P., Moosmüller, H. and Wold, C. E.: Strong spectral variation of biomass smoke light absorption and single scattering albedo observed with a novel dual-

wavelength photoacoustic instrument, J. Geophys. Res. Atmos., doi:10.1029/2007JD009699, 2008.

Liljegren, J. C., Clothiaux, E. E., Mace, G. G., Kato, S. and Dong, X.: A new retrieval for cloud liquid water path using a ground-based microwave radiometer and measurements of cloud temperature, J. Geophys. Res. Atmos., doi:10.1029/2000JD900817, 2001.

Liu, H. J., Zhao, C. S., Nekat, B., Ma, N., Wiedensohler, A., van Pinxteren, D., Spindler, G., Müller, K., and Herrmann, H.: Aerosol hygroscopicity derived from size-segregated chemical composition and its parameterization in the North China Plain, Atmos. Chem. Phys., 14, 2525-2539, https://doi.org/10.5194/acp-14-2525-2014, 2014.

Liu, J. and Li, Z.: Estimation of cloud condensation nuclei concentration from aerosol optical quantities: Influential factors and uncertainties, Atmos. Chem. Phys., doi:10.5194/acp-14-471-2014, 2014.

Liu, Y., Wu, W., Jensen, M. P. and Toto, T.: Relationship between cloud radiative forcing, cloud fraction and cloud albedo, and new surface-based approach for determining cloud albedo, Atmos. Chem. Phys., doi:10.5194/acp-11-7155-2011, 2011.

Logan, T., Xi, B., Dong, X., Obrecht, R., Li, Z. and Cribb, M.: A study of Asian dust plumes using satellite, surface, and aircraft measurements during the INTEX-B field experiment, J. Geophys. Res. Atmos., doi:10.1029/2010JD014134, 2010.

Logan, T., Xi, B., Dong, X., Li, Z., and Cribb, M.: Classification and investigation of Asian aerosol absorptive properties, Atmos. Chem. Phys., 13, 2253-2265, https://doi.org/10.5194/acp-13-2253-2013, 2013.

Logan, T., Xi, B. and Dong, X.: Aerosol properties and their influences on marine boundary layer cloud condensation nuclei at the ARM mobile facility over the Azores, J. Geophys. Res., doi:10.1002/2013JD021288, 2014.

Logan, T., Dong, X. and Xi, B.: Aerosol properties and their impacts on surface CCN at the ARM Southern Great Plains site during the 2011 Midlatitude Continental Convective Clouds Experiment, Adv. Atmos. Sci., doi:10.1007/s00376-017-7033-2, 2018.

Long, C. N. and Ackerman, T. P.: Identification of clear skies from broadband pyranometer measurements and calculation of downwelling shortwave cloud effects, J. Geophys. Res. Atmos., doi:10.1029/2000JD900077, 2000.

Long, C. N. and Turner, D. D.: A method for continuous estimation of clear-sky downwelling longwave radiative flux developed using ARM surface measurements, J. Geophys. Res. Atmos., doi:10.1029/2008JD009936, 2008.

Mace, G. G., Benson, S., Sonntag, K. L., Kato, S., Min, Q., Minnis, P., Twohy, C. H., Poellot, M., Dong, X., Long, C., Zhang, Q. and Doelling, D. R.: Cloud radiative forcing at the Atmospheric Radiation Measurement Program Climate Research Facility: 1. technique, validation, and comparison to satellite-derived diagnostic quantities, J. Geophys. Res. Atmos., doi:10.1029/2005JD005921, 2006.

Massling, A., Stock, M., Wehner, B., Wu, Z. J., Hu, M., Brüggemann, E., Gnauk, T., Herrmann, H. and Wiedensohler, A.: Size segregated water uptake of the urban submicrometer aerosol in Beijing, Atmos. Environ., doi:10.1016/j.atmosenv.2008.06.003, 2009.

McComiskey, A. and Feingold, G.: Quantifying error in the radiative forcing of the first aerosol indirect effect, Geophys. Res. Lett., doi:10.1029/2007GL032667, 2008.

McComiskey, A, Feingold, G., Frisch, A. S., Turner, D. D., Miller, M., Chiu, J. C., Min, Q., and Ogren, J.: An assessment of aerosol-cloud interactions in marine stratus clouds based on surface remote sensing, J. Geophys. Res., 114, D09203, doi:10.1029/2008JD011006, 2009.

McFiggans, G., Artaxo, P., Baltensperger, U., Coe, H., Facchini, M. C., Feingold, G., Fuzzi, S., Gysel, M., Laaksonen, A., Lohmann, U., Mentel, T. F., Murphy, D. M., O'Dowd, C. D., Snider, J. R., and Weingartner, E.: The effect of physical and chemical aerosol properties on warm cloud droplet activation, Atmos. Chem. Phys., 6, 2593-2649, https://doi.org/10.5194/acp-6-2593-2006, 2006.

Miles, N. L., Verlinde, J. and Clothiaux, E. E.: Cloud Droplet Size Distributions in Low-Level Stratiform Clouds, J. Atmos. Sci., doi:10.1175/1520-0469(2000)057<0295:cdsdil>2.0.co;2, 2002.

24

Painemal, D. and Zuidema, P.: The first aerosol indirect effect quantified through airborne remote sensing during VOCALS-REx, Atmos. Chem. Phys., 13, 917-931, https://doi.org/10.5194/acp-13-917-2013, 2013.

Parworth, C., Fast, J., Mei, F., Shippert, T., Sivaraman, C., Tilp, A., Watson, T. and Zhang, Q.: Long-term measurements of submicrometer aerosol chemistry at the Southern Great Plains (SGP) using an Aerosol Chemical Speciation Monitor (ACSM), Atmos. Environ., doi:10.1016/j.atmosenv.2015.01.060, 2015.

Rose, D., Nowak, A., Achtert, P., Wiedensohler, A., Hu, M., Shao, M., Zhang, Y., Andreae, M. O., and Pöschl, U.: Cloud condensation nuclei in polluted air and biomass burning smoke near the mega-city Guangzhou, China – Part 1: Size-resolved measurements and implications for the modeling of aerosol particle hygroscopicity and CCN activity, Atmos. Chem. Phys., 10, 3365-3383, https://doi.org/10.5194/acp-10-3365-2010, 2010.

Rose, D., Gunthe, S. S., Su, H., Garland, R. M., Yang, H., Berghof, M., Cheng, Y. F., Wehner, B., Achtert, P., Nowak, A., Wiedensohler, A., Takegawa, N., Kondo, Y., Hu, M., Zhang, Y., Andreae, M. O., and Pöschl, U.: Cloud condensation nuclei in polluted air and biomass burning smoke near the mega-city Guangzhou, China – Part 2: Size-resolved aerosol chemical composition, diurnal cycles, and externally mixed weakly CCN-active soot particles, Atmos. Chem. Phys., 11, 2817-2836, https://doi.org/10.5194/acp-11-2817-2011, 2011.

Russell, P. B., Bergstrom, R. W., Shinozuka, Y., Clarke, A. D., DeCarlo, P. F., Jimenez, J. L., Livingston, J. M., Redemann, J., Dubovik, O., and Strawa, A.: Absorption Angstrom Exponent in AERONET and related data as an indicator of aerosol composition, Atmos. Chem. Phys., 10, 1155-1169, https://doi.org/10.5194/acp-10-1155-2010, 2010.

Schmeisser, L., Andrews, E., Ogren, J. A., Sheridan, P., Jefferson, A., Sharma, S., Kim, J. E., Sherman, J. P., Sorribas, M., Kalapov, I., Arsov, T., Angelov, C., Mayol-Bracero, O. L., Labuschagne, C., Kim, S.-W., Hoffer, A., Lin, N.-H., Chia, H.-P., Bergin, M., Sun, J., Liu, P., and Wu, H.: Classifying aerosol type using in situ surface spectral aerosol optical properties, Atmos. Chem. Phys., 17, 12097-12120, https://doi.org/10.5194/acp-17-12097-2017, 2017.

Atmospheric
Chemistry
and Physics
Discussions

Schuster, G. L., Dubovik, O., Holben, B. N. and Clothiaux, E. E.: Inferring black carbon content and specific absorption from Aerosol Robotic Network (AERONET) aerosol retrievals, J. Geophys. Res. D Atmos., doi:10.1029/2004JD004548, 2005.

Schuster, G. L., Dubovik, O. and Holben, B. N.: Angstrom exponent and bimodal aerosol size distributions, J. Geophys. Res. Atmos., doi:10.1029/2005JD006328, 2006.

Sekiguchi, M.: A study of the direct and indirect effects of aerosols using global satellite data sets of aerosol and cloud parameters, J. Geophys. Res., doi:10.1029/2002jd003359, 2003.

Sena, E. T., McComiskey, A., and Feingold, G.: A long-term study of aerosol–cloud interactions and their radiative effect at the Southern Great Plains using ground-based measurements, Atmos. Chem. Phys., 16, 11301-11318, https://doi.org/10.5194/acp-16-11301-2016, 2016.

Seinfeld, J. H. and Pandis, S. N.: Atmospheric chemistry and physics: From air pollution to climate change, 2 ed., John Wiley & Sons, Inc., 1225 pp., 2006.

Shinozuka, Y., Clarke, A. D., DeCarlo, P. F., Jimenez, J. L., Dunlea, E. J., Roberts, G. C., Tomlinson, J. M., Collins, D. R., Howell, S. G., Kapustin, V. N., McNaughton, C. S., and Zhou, J.: Aerosol optical properties relevant to regional remote sensing of CCN activity and links to their organic mass fraction: airborne observations over Central Mexico and the US West Coast during MILAGRO/INTEX-B, Atmos. Chem. Phys., 9, 6727-6742, https://doi.org/10.5194/acp-9-6727-2009, 2009.

Sorooshian, A., Feingold, G., Lebsock, M. D., Jiang, H. and Stephens, G. L.: Deconstructing the precipitation susceptibility construct: Improving methodology for aerosol-cloud precipitation studies, J. Geophys. Res. Atmos., doi:10.1029/2009JD013426, 2010.

Stein, A. F., Draxler, R. R, Rolph, G. D., Stunder, B. J. B., Cohen, M. D., and Ngan, F.: NOAA's HYSPLIT atmospheric transport and dispersion modeling system, Bull. Amer. Meteor. Soc., 10 96, 2059-2077, http://dx.doi.org/10.1175/BAMS-D-14-00110.1, 2015.

Su, W., Loeb, N. G., Xu, K. M., Schuster, G. L. and Eitzen, Z. A.: An estimate of aerosol indirect effect from satellite measurements with concurrent meteorological analysis, J. Geophys. Res. Atmos., doi:10.1029/2010JD013948, 2010.

Tian, P., Cao, X., Zhang, L., Sun, N., Sun, L., Logan, T., Shi, J., Wang, Y., Ji, Y., Lin, Y., Huang, Z., Zhou, T., Shi, Y., and Zhang, R.: Aerosol vertical distribution and optical properties over China from long-term satellite and ground-based remote sensing, Atmos. Chem. Phys., 17, 2509-2523, https://doi.org/10.5194/acp-17-2509-2017, 2017.

5   Troyan, D.: Merged Sounding Value-Added Product, Tech. Rep., DOE/SC-ARM/TR-087, 2012.

Twohy, C. H., Anderson, J. R., Toohey, D. W., Andrejczuk, M., Adams, A., Lytle, M., George, R. C., Wood, R., Saide, P., Spak, S., Zuidema, P., and Leon, D.: Impacts of aerosol particles on the microphysical and radiative properties of stratocumulus clouds over the southeast

10   Pacific Ocean, Atmos. Chem. Phys., 13, 2541-2562, https://doi.org/10.5194/acp-13-2541-2013, 2013.

Twomey, S.: The Influence of Pollution on the Shortwave Albedo of Clouds, J. Atmos. Sci., doi:10.1175/1520-0469(1977)034<1149:TIOPOT>2.0.CO;2, 1977.

Vavrus, S.: An alternative method to calculate cloud radiative forcing: Implications for

15   quantifying cloud feedbacks, Geophys. Res. Lett., doi:10.1029/2005GL024723, 2006.

Wang, J., Cubison, M. J., Aiken, A. C., Jimenez, J. L., and Collins, D. R.: The importance of aerosol mixing state and size-resolved composition on CCN concentration and the variation of the importance with atmospheric aging of aerosols, Atmos. Chem. Phys., 10, 7267-7283, https://doi.org/10.5194/acp-10-7267-2010, 2010.

20   Wang, Y., Fan, J., Zhang, R., Leung, L. R. and Franklin, C.: Improving bulk microphysics parameterizations in simulations of aerosol effects, J. Geophys. Res. Atmos., doi:10.1002/jgrd.50432, 2013.

Wang, Y., Vogel, J. M., Lin, Y., Pan, B., Hu, J., Liu, Y., Dong, X., Jiang, J. H., Yung, Y. L. and Zhang, R.: Aerosol microphysical and radiative effects on continental cloud ensembles,

25   Adv. Atmos. Sci., doi:10.1007/s00376-017-7091-5, 2018a.

Wang, Y., Ma, P. L., Peng, J., Zhang, R., Jiang, J. H., Easter, R. C. and Yung, Y. L.: Constraining Aging Processes of Black Carbon in the Community Atmosphere Model Using Environmental Chamber Measurements, J. Adv. Model. Earth Syst., doi:10.1029/2018MS001387, 2018b.

Widener, K, Bharadwaj, N, and Johnson, K: Ka-Band ARM Zenith Radar (KAZR) Instrument Handbook. United States: N. p., Web. doi:10.2172/1035855, 2012.

Xi, B., Dong, X., Minnis, P. and Khaiyer, M. M.: A 10 year climatology of cloud fraction and vertical distribution derived from both surface and GOES observations over the DOE ARM SPG site, J. Geophys. Res. Atmos., doi:10.1029/2009JD012800, 2010.

Zhang, Q., Meng, J., Quan, J., Gao, Y., Zhao, D., Chen, P., and He, H.: Impact of aerosol composition on cloud condensation nuclei activity, Atmos. Chem. Phys., 12, 3783-3790, https://doi.org/10.5194/acp-12-3783-2012, 2012.

Zhao, C., Qiu, Y., Dong, X., Wang, Z., Peng, Y., Li, B., Wu, Z. and Wang, Y.: Negative Aerosol-Cloud re Relationship from Aircraft Observations Over Hebei, China, Earth Sp. Sci., doi:10.1002/2017EA000346, 2018.

Table 1. Dates and time periods of selected low-level stratus cloud cases and their airmass sources

Date	Start Time (UTC)	End Time (UTC)	Airmass Source
4 Jan 2007	15:00	22:30	S
5 Jan 2007	14:00	18:10	S
13 Feb 2007	17:00	22:30	N
26 Apr 2007	14:00	17:30	NE
21 Nov 2007	13:20	18:15	N
14 Feb 2009	15:15	17:35	NW
12 May 2009	16:55	20:05	SE
19 Dec 2009	14:40	19:35	NW
21 Jan 2010	15:25	22:30	N
16 Mar 2010	15:00	20:00	N
29 Dec 2010	16:00	18:35	SE
26 Mar 2011	16:35	23:55	NE
13 May 2011	12:25	18:20	N
4 Feb 2012	16:40	21:10	NE
8 Feb 2012	14:30	19:45	N
10 Feb 2012	17:15	19:50	NW

Airmass sources denote the relative directions from where the airmasses advected to SGP.
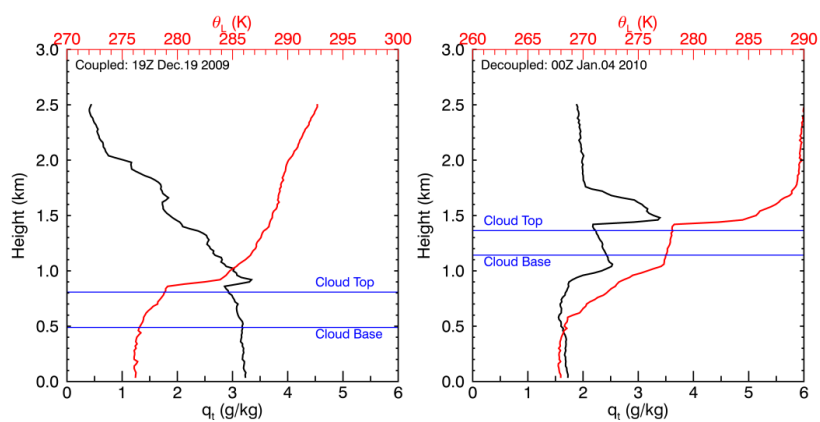
Figure 1. Vertical profiles of liquid water potential temperature (θ_L) and total water mixing ratio (q_t) for coupled (a) and decoupled (b) boundary layer conditions. Blue lines denote cloud top and base heights, respectively.
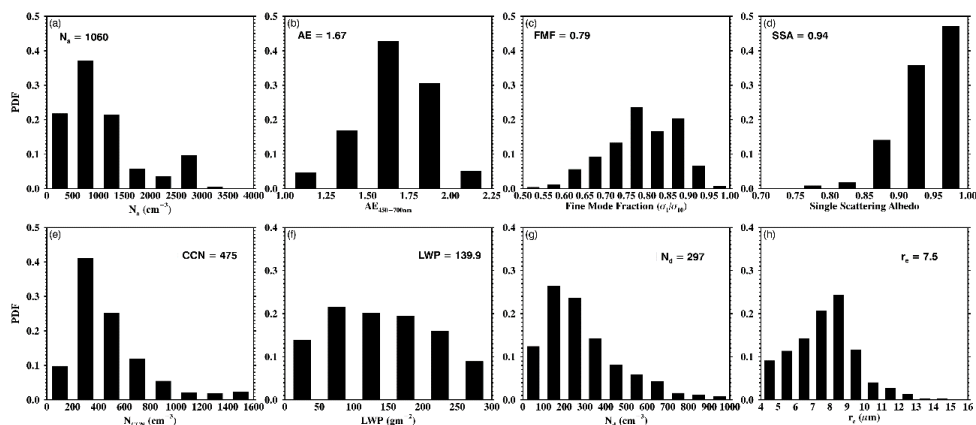
Figure 2. Probability distribution functions (PDFs) and mean values of low-level stratus cloud and aerosol properties for all cases: (a) total aerosol number concentration (Na); (d) single scattering albedo at 450 nm (SSA); (b) Ångström Exponent (AE) derived from 450 nm to 700 nm nephelometer measurements; (c) fine mode fraction at 550 nm; (e) cloud condensation nuclei number concentration (NCCN); (f) liquid water path (LWP); (g) cloud droplet number concentration (Nd); (h) cloud droplet effective radius (re).
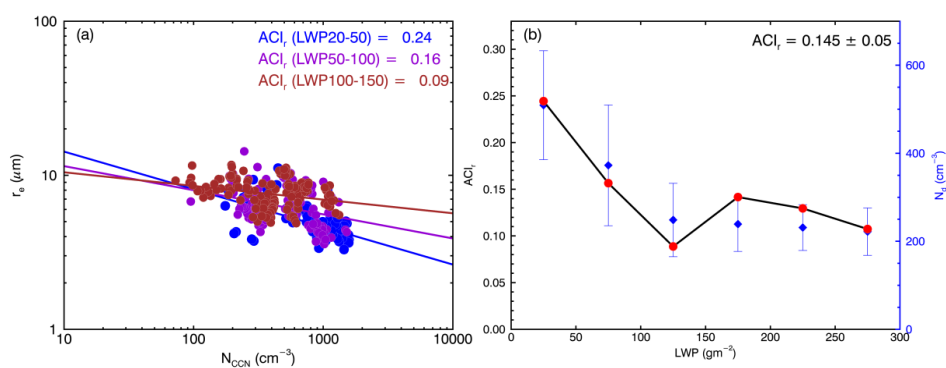
Figure 3. ACI_r derived from (a) r_e to N_{CCN} in following three LWP bins: 20-50 gm^{-2} (blue), 50-100 gm^{-2} (purple), 100-150 gm^{-2} (dark red) and (b) Relationship of ACI_r (red dot, left ordinate) and N_d (blue diamond, right ordinate) to binned LWP. Blue whiskers denote one standard deviation for each bin.
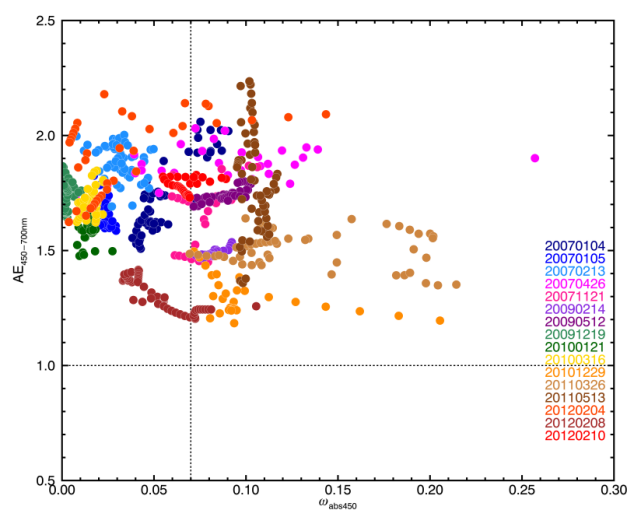
Figure 4. Angstrom Exponent ($AE_{450-700nm}$) and single scattering Co-albedo ω_{abs450} of all samples with color coded for each case.
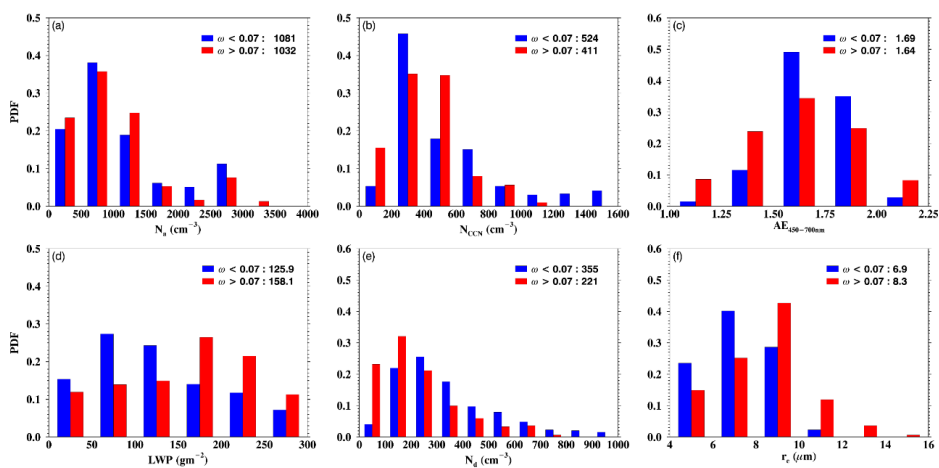
Figure 5. Aerosol and cloud properties under the strongly absorptive (in red) and weakly absorptive (in blue) aerosol regimes. PDFs and mean values of (a) N_a; (b) N_{CCN}; (c) $AE_{450-700nm}$; (d) LWP; (e) N_d; (f) r_e.
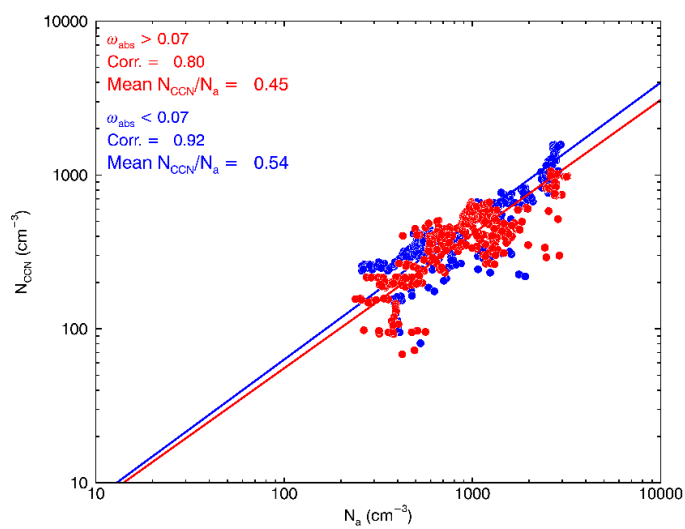
Atmospheric
Chemistry
and Physics
Discussions

Figure 6. Relationship between N_{CCN} and N_a under the strongly absorptive aerosol regime (in red) and weakly absorptive aerosol regime (in blue).
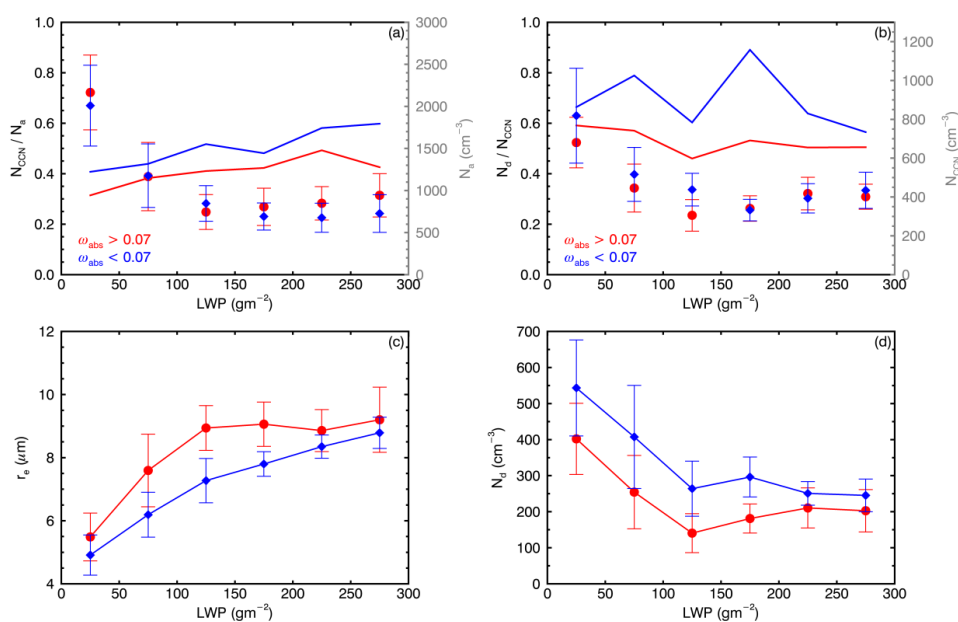
Figure 7. (a) N_a (dot) and the ratio of N_{CCN} to N_a (line); (b) N_{CCN} (dot) and the ratio of N_d to N_{CCN} (line); (c) r_e; and (d) N_d as a function of LWP under strongly absorptive (in red) and weakly absorptive (in blue) aerosol regimes. Whiskers denote one standard deviation for each bin.
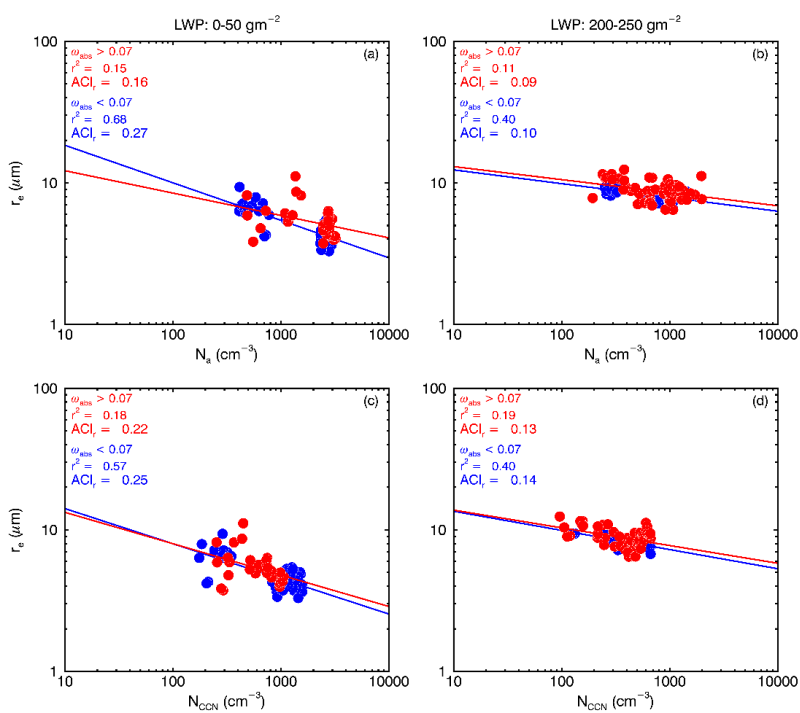
Figure 8. ACI_r under the strongly absorptive (in red) and weakly absorptive (in blue) aerosol regimes at two LWP bins: 0-50 g m^{-2} (a, c) and 200-250 g m^{-2} (b, d). Top panel denotes r_e as a function of N_a (a, b); bottom panel denotes r_e as a function of N_{CCN} (c, d).
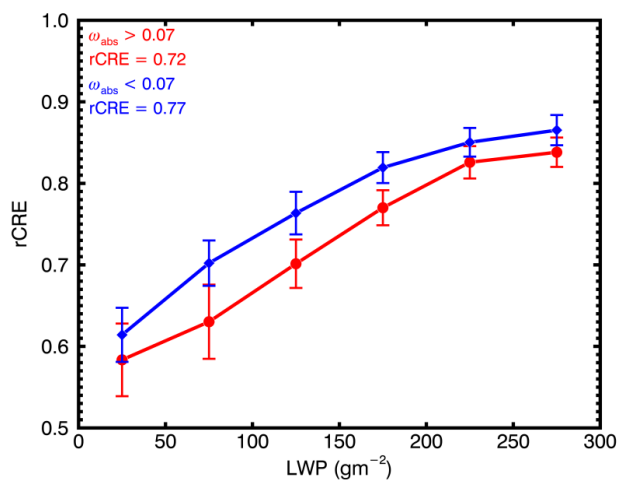
Figure 9. Relative Cloud Radiative Effect (rCRE) as a function of liquid water path (LWP) under strongly absorptive (in red) and weakly absorptive (in blue) aerosol regimes. Whiskers denote one standard deviation for each bin.